



1 **Observed global ocean phytoplankton phenology indices.**

2 Sarah-Anne Nicholson¹, Thomas J. Ryan-Keogh¹, Sandy J. Thomalla^{1,2}, Nicolette Chang^{1,5},
3 Marié E. Smith^{3,4}

4 ¹Southern Ocean Carbon-Climate Observatory, CSIR, Cape Town, South Africa

5 ²Marine and Antarctic Research Centre for Innovation and Sustainability, University of Cape Town, Cape Town,
6 South Africa

7 ³Coastal Systems and Earth Observation Research Group, CSIR, Cape Town, South Africa

8 ⁴Department of Oceanography, University of Cape Town, Cape Town, South Africa

9 ⁵Global Change Institute, University of the Witwatersrand, Johannesburg, South Africa

10

11 *Correspondence to:* Sarah-Anne Nicholson (snicholson@csir.co.za)

12

13 **Abstract**

14 Phytoplankton bloom phenology is an important indicator for the monitoring and management of marine resources
15 and the assessment of climate change impacts on ocean ecosystems. Despite its relevance, there is no long-term
16 and sustained observational phytoplankton phenological product available for global ocean implementation. The
17 data product presented here addresses this need through the development of phenological detection algorithms
18 (including among other seasonal metrics, the bloom initiation, termination, duration, and amplitude timing) using
19 satellite derived chlorophyll-a data from the Ocean Colour Climate Change Initiative. This product provides the
20 phenology output from three widely used bloom detection algorithms at three different spatial resolutions (4, 9
21 and 25 km) allowing for both regional and global-scale applications. In this study, the mean global phenology is
22 characterised according to the three phenological detection methods and the different resolutions, which are
23 compared to one another. In general, there is good agreement between the detection methods and between different
24 resolutions on global scales. Regional differences are evident in coastal domains (particularly for resolution) and
25 in regions with strong transitions between phytoplankton seasonal characteristics. This product can be used
26 towards the development of national and global biodiversity assessments, pelagic ecosystem mapping and for
27 monitoring change in climate sensitive regions relevant for ecosystem services. The dataset is published in the
28 Zenodo repository under the following DOIs, 4 km: <https://doi.org/10.5281/zenodo.8402932>. 9 km:
29 <https://doi.org/10.5281/zenodo.8402847> and 25 km: <https://doi.org/10.5281/zenodo.8402823> (Nicholson et al.,
30 2023a, b, c) and will be updated regularly.



31 **1 Introduction**

32 The seasonal proliferation of phytoplankton across the world's ocean is a ubiquitous signal visible from space,
33 and one that plays a crucial role in the Earth system. Phytoplankton "blooms" capture 30-50 billion metric tons of
34 carbon annually, representing almost half of the total carbon uptake by all plant matter (Falkowski, 1994;
35 Longhurst et al., 1995; Field et al., 1998; Carr et al., 2006; Buitenhuis et al., 2013). Their key role in driving the
36 strength and efficiency of the biological carbon pump, the transfer of atmospheric carbon to the deep ocean
37 interior, is a crucial component of the global carbon cycle and instrumental in the assessment of climate feedbacks
38 and change (Henson et al., 2011; Devries, 2022). Phytoplankton also mediate climate through the production of
39 important atmospheric trace gases such as nitrous oxide, a potent greenhouse gas, and volatile organic carbons
40 such as dimethyl sulphide, that have a significant impact on cloud formation and global albedo (Charlson et al.,
41 1987; Korhonen et al., 2008; McCoy et al., 2015; Park et al., 2021). As the foundation of the marine food chain,
42 phytoplankton are critical to supporting higher trophic levels and a lucrative fisheries industry that impacts global
43 food security (Stock et al., 2017; Gittings et al., 2021). There is an enormous benefit to society in being able to
44 predict ecosystem responses to environmental change, by providing the knowledge necessary for competent
45 decision-making. As such understanding, characterising and accurately predicting changes in the annual cycle of
46 phytoplankton blooms provides an essential tool for managing marine resources and for predicting future climate
47 change impacts (Tweddle et al., 2018; Thomalla et al., 2023).

48

49 Phytoplankton phenology refers to the timing of seasonal activities of phytoplankton biomass and is used widely
50 as an indicator to monitor phytoplankton blooms. Adjustments in the characteristics of phenology typically reflect
51 alterations in ecosystem function that may be linked to environmental pressures such as climate change (Racault
52 et al., 2012; Henson et al., 2018; Thomalla et al., 2023). Key phenological phases of phytoplankton bloom
53 development include: the time of initiation, the time of maximum concentration (amplitude), the time of
54 termination and duration as the time between initiation and termination. These phytoplankton bloom phases are
55 typically driven by seasonal changes in physical forcing (such as incoming solar radiation, water column mixing
56 and nutrient depletion), which are generally linked to large-scale climate drivers (Racault et al., 2012; Thomalla
57 et al., 2023). The timing of the bloom initiation and amplitude is particularly critical for efficient trophic energy
58 transfer, which can be impacted negatively through trophic decoupling. For example, mismatches between bloom
59 timing and zooplankton grazing can lead to suboptimal food conditions for higher trophic levels which in turn has
60 been linked to the collapse of crucial fisheries (Cushing, 1990; Koeller et al., 2009; Seyboth et al., 2016; Stock et
61 al., 2017). Bloom duration impacts the amount of biomass being generated within a season that can be exported
62 to the ocean's interior or transferred to higher trophic levels via the marine food web and can thus play a more
63 important role than bloom magnitude (Barnes, 2018; Rogers et al., 2020). Bloom timing has also been shown to
64 influence the seasonal cycles of CO₂ uptake, primary production and the efficiency of carbon export and storage
65 (Lutz et al., 2007; Bennington et al., 2009; Palevsky & Quay, 2017; Boot et al., 2023)

66

67 Current generation Earth System Models (ESMs) show that phytoplankton phenology is changing and will
68 continue to change in response to a warming and more stratified ocean (Henson et al., 2018; Yamaguchi et al.,
69 2022). For example, blooms are predicted to initiate later in the mid-latitudes and earlier at high and low latitudes



70 by ~5 days per decade by the end of the century (Henson et al., 2018). But what about changes in bloom phenology
71 in the contemporary period? Satellite-based ocean colour remote sensing, which provides estimates of
72 chlorophyll-a (chl-a) concentrations (a proxy for phytoplankton abundance), is the only observational capability
73 that can provide synoptic views of upper ocean phytoplankton characteristics at high spatial and temporal
74 resolution (~1 km, ~daily) and high temporal extent (global scales, for years to decades). In many cases, these are
75 the only systematic observations available for chronically under-sampled marine systems such as the polar oceans.
76 In 1997, the first global ocean colour observing satellite (SeaWiFS) was launched and these observations have
77 been sustained through a successive series of additional ocean colour satellites (MODIS, MERIS, VIIRS, OLCI).
78 These have all been merged by the European Space Agency into the Ocean Colour Climate Change Initiative
79 (OC-CCI) data product, which provides ~25 years of ocean colour data for climate change assessment
80 (Sathyendranath et al., 2019). The estimation of phytoplankton phenology from this data product on a global scale
81 can provide important information of the rates of change in key indices for comparison to those derived from
82 ESM's. For example, using 25 years of satellite-derived chl-a (1997-2022), (Thomalla et al., 2023) recently
83 revealed that large regions of the Southern Ocean expressed significant trends in phenological indices that were
84 typically much larger (e.g. <math>< 50 \text{ days decade}^{-1}</math>) than those reported in previous climate modelling studies (<math>< 5-10</math>
85 days decade^{-1}). Thomalla et al. (2023) conclude, that seasonal adjustments of this magnitude at the base of the
86 food web may impact the nutritional stress, reproductive success, and survival rates of larger marine species (e.g.,
87 seals, seabirds, and humpback whales), in particular if they are unable to synchronise their feeding and breeding
88 patterns with that of their food supplies. A similar analysis using these key phytoplankton metrics applied to the
89 global ocean will reveal regional sensitivities of ecosystems to change with important implications for ecosystem
90 function and climate. There is also a need to have a global phytoplankton phenology product such as this annually
91 updated to allow for the continuous monitoring and assessment of the seasonal adjustments of phytoplankton on
92 global scales (in addition to continued benchmarking for ESMs). These assessments of the sensitivity of key
93 ecosystems to change are relevant for effective marine management programs and early detection of
94 vulnerabilities in key regions, e.g., those necessary for sustaining fisheries. In addition, a phenology data product
95 such as this can provide a useful aid for the planning of oceanographic research campaigns among many other
96 applications.

97

98 In this paper, we present a new data product consisting of global phytoplankton phenological indicators (including
99 among other metrics bloom initiation, termination, amplitude, and duration) computed using three different
100 gridded resolutions (4, 9 and 25 km) and with three different methodologies of determining key metrics. The data
101 product is currently available from 1997 until 2022 and will be updated annually and in sync with any version
102 updates of the OC-CCI chl-a data product.

103 **2 Methodology**

104 **2.1 Data and pre-processing**



105 Satellite-derived chl-a concentrations (mg m^{-3}) were obtained from the European Space Agency, from OC-CCI
106 (<https://esa-oceancolour-cci.org>; (Sathyendranath et al., 2019) at 4 km and 8-day resolution. The latest available
107 OC-CCI product (version v6.0, released on 04/11/2022) is used in this present study. This version marks a
108 substantial change to previous versions (e.g., v5.0, see Sathyendranath et al., 2021) in that it incorporates Sentinel
109 3B OLCI data, the MERIS-4th reprocessing dataset, upgraded Quasi-Analytical algorithm (QAAv6) and the
110 exclusion of MODIS and VIIRS data after 2019 (refer to D4.2 - Product User Guide for v6.0 Dataset from
111 <https://climate.esa.int/en/projects/ocean-colour/key-documents/>). Data provided by OC-CCI covered the period
112 from 29/08/1997 – 27/12/2022 for the global ocean ($90^{\circ}\text{N} - 90^{\circ}\text{S}$ and $180^{\circ}\text{E} - 180^{\circ}\text{W}$).

113

114 The phenological indices described below are calculated using three horizontal resolutions in surface chl-a, the
115 native 4 km resolution as provided by OC-CCI and a regridded 9 km and 25 km horizontal resolution. The 4 km
116 and 9 km resolutions are considered important for smaller-scale regional needs such as coastal applications and
117 field campaigns. The 25 km resolution is the most computationally efficient for users to work with, it results in a
118 reduction of missing data and is useful for global open-ocean applications. For the 9 km and 25 km resolutions,
119 chl-a is regridded onto a regular grid through bilinear interpolation using the xESMF Python package (Zhuang et
120 al., 2023). In all resolutions for phenological detection, data gaps were reduced further by applying a linear
121 interpolation scheme in sequential steps of longitude, latitude, and time (Racault et al., 2014). A two-point limit
122 (e.g., the maximum number of consecutive empty grid cells to fill) is chosen for the interpolation to avoid
123 overfilling of regions that contain larger coherent data gaps. We further apply a 3 time-step (24 days) rolling mean
124 along the time dimension to avoid any outliers that may result in fake detection points. However, for the Seasonal
125 Cycle Reproducibility (SCR) computations only interpolation (time, lat and lon) is carried out, this is discussed
126 further below.

127 **2.2 Phenological Indices and Detection**

128 Phytoplankton blooms typically manifest as a seasonal cycle, with a bloom initiation that identifies the timing of
129 the ramp up in phytoplankton growth and biomass accumulation followed by bloom peaks within the growing
130 season (which could be multiple) and finally the bloom termination, which defines the end of the growing season.
131 The phenological indices applied here are based on those applied to the SO in (Thomalla et al., 2023). To calculate
132 the phenological indices for initiation and termination, we apply three main detection methods used by the
133 community (refer to Brody et al., 2013) which are detailed below (iii and iv). Each detection method has its
134 strengths and weaknesses, and therefore the choice of method for application can be determined by the user needs,
135 which are elaborated on in (Brody et al., 2013). These methods were chosen over other approaches (e.g., Rolinski
136 et al., 2007; Platt et al., 2009) due to the method's suitability for estimates across global scales as it is capable of
137 encompassing a wide range of different shapes in phytoplankton blooms (Racault et al., 2012). In this data product,
138 all three approaches are provided globally at all three resolutions. Below we outline the series of steps
139 implemented for estimating the global phenological indices and provide an accompanying flow chart (Figure 1)
140 to illustrate the succession of steps being implemented. In addition, we provide some example applications at four
141 key observing stations (Figure A1) to facilitate a visualisation of the derived phenological indices from four annual
142 time series.



143

144 (i) Bloom maximum climatology: The climatological peak (maximum amplitude) of the bloom was identified as
145 the local maximum in chl-a occurring within each grid cell's 25-year climatology. This approach was necessary
146 because the timing of bloom events varies globally, i.e., southern hemisphere blooms typically occur during austral
147 spring - summer (September - February), while northern hemisphere blooms occur in boreal spring - summer
148 (April - August)(Racault et al., 2012). Furthermore, both hemisphere tropics tend to be approximately 6 months
149 out of phase with both hemisphere higher latitude regions. As such, it would be inappropriate to use a fixed date
150 period (or "bloom slice" see below) to identify bloom occurrence on global scales. Instead, for each grid cell we
151 calculate the 8-day mean climatology. The date of the maximum climatological bloom for each pixel is then used
152 to centre the timing of the phenology detection algorithms described below.

153

154 (ii) Identification of bloom peaks: For every pixel on a year-by-year basis we take the climatological bloom
155 maximum peak ± 6 months and determine the date and magnitude of the bloom maximum peak for each year. To
156 ensure that seasonal blooms with more than one peak could be accounted for, multiple bloom peaks were defined
157 as a second, third, or n^{th} local maxima where the chl-a concentration reached at least 75% of the amplitude of the
158 bloom maximum peak magnitude and were a minimum of 24 days (i.e., 3 x 8 day time intervals) away from the
159 bloom maximum peak for that year. These additional peaks were found within ± 6 months of the maximum peak.
160 An example of such a multi-peak bloom detection is provided in Figure 1 and Figure A1c. The additional peaks
161 were identified with the Python SciPy (Virtanen et al., 2020) function 'find_peaks'.

162

163 (iii) The 'bloom slice': The bloom slice, used to find the bloom initiation and termination dates, is identified for
164 each pixel as the 6 month time span preceding and following from the maximum bloom peak (ii). Or in the case
165 of multi-modal blooms, 6-months preceding the first and following the last peak respectively.

166

167 (iv) Bloom initiation: The bloom initiation date for each bloom slice as described in (iii) is calculated as the first
168 date before either the bloom maximum, or the first peak in the event of multi-modal blooms, according to the
169 following thresholds:

170 1. *Biomass-based threshold method (TS)*: First determine the range as the difference in chl-a concentration
171 between the bloom maximum and preceding minimum. Then identify the bloom initiation as the first
172 date that the chl-a concentration was greater than the minimum chl-a concentration plus 5% of the chl-a
173 range.

174 2. *Cumulative biomass-based threshold method (CS)*: First remove any values preceding the bloom slice
175 minimum chl-a concentration and any values greater than 3 times the median of the bloom slice, before
176 calculating the cumulative sum of chl-a. Then identify the first date that the chl-a concentration was
177 greater than 15% of the total cumulative chl-a concentration.

178 3. *The rate of change method (RC)*: First determine the rate of change of the bloom slice and then identify
179 the first date that the chl-a rate of change was greater than 15% of the median rate of change in chl-a
180 concentration.

181



182 (v) Bloom termination: The bloom termination date for each bloom slice was similarly calculated as the first date
183 after the bloom maximum, or the last peak in the event of multi-modal blooms, according to the following
184 thresholds:

- 185 1. *TS*: the first date that the chl-a concentration was less than the minimum chl-a concentration plus 5% of
186 the chl-a range.
- 187 2. *CS*: the first date that the chl-a concentration was less than 15% of the total cumulative chl-a
188 concentration.
- 189 3. *RC*: the first date that chl-a rate of change was less than 15% of the median rate of change in chl-a
190 concentration.

191

192 (vi) Bloom duration: The bloom duration was calculated as the number of days between the bloom initiation and
193 termination dates. This is applied to each phenological detection method described above (*TS*, *CS* and *RC*).

194

195 (vii) Integrated and mean bloom chl-a: The seasonally integrated bloom chl-a was calculated using the NumPy
196 (Harris et al., 2020) trapezoidal function as the chl-a concentration integrated between the bloom initiation and
197 termination dates. The seasonal mean chl-a was calculated as the average chl-a between the bloom initiation and
198 termination dates. These are applied to each of the three phenological detection methods described above (*TS*, *CS*
199 and *RC*).

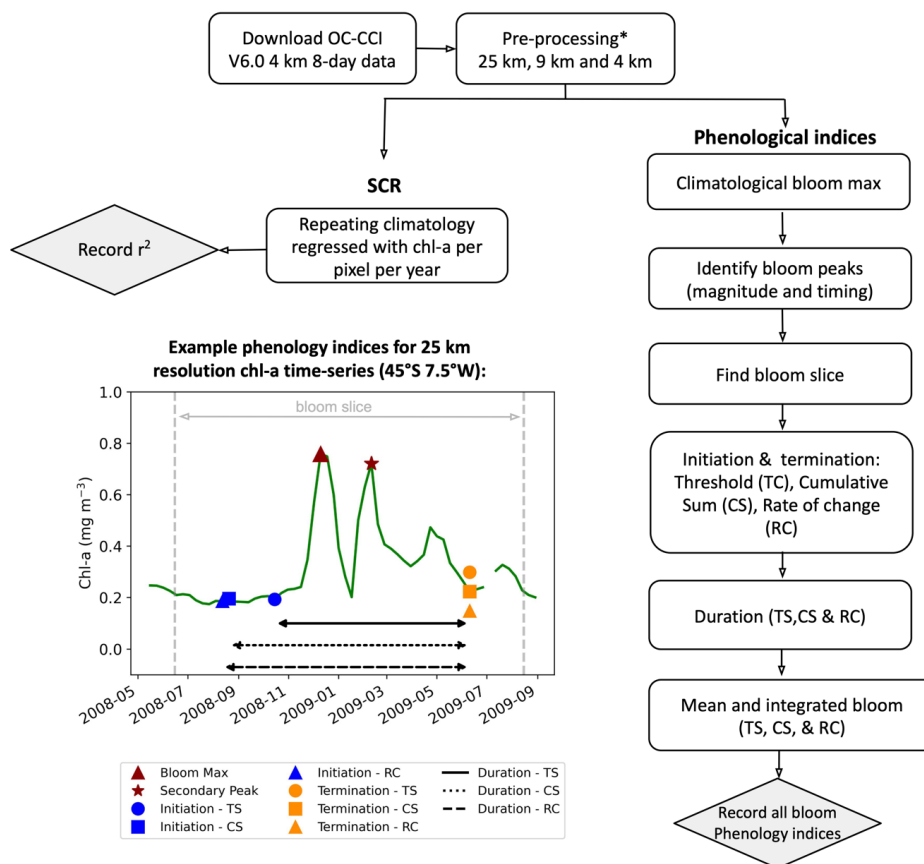
200

201 (viii) *SCR*: The variance of the seasonal cycle was calculated as defined in Thomalla et al., (2023), where the *SCR*
202 is the Pearson's correlation coefficient of the annual seasonal cycle correlated against the climatological mean
203 seasonal cycle. A value of 100% is indicative of an annual seasonal cycle that is a perfect repetition of the
204 climatological mean, while a value of 0% means that there is no annually reproducible mean seasonal cycle.
205 Unlike for phenological indices i-vii, for *SCR* the original OC-CCI v6.0 data were used for the three different grid
206 resolutions, however with only spatial-temporal interpolation for gap filling and no rolling mean to avoid
207 smoothing out temporal variability. For *SCR* for each pixel the bloom slice is restricted to 12 months (i.e., January
208 to December).

209

210 To generate climatological means we used the Python SciPy function 'circmean' which calculates circular means
211 for samples in a range. For example, we need to avoid a situation where the mean bloom initiation between a year
212 with a bloom in December (e.g., day of year = 350) and a year with a bloom in January (e.g., day of year = 20) is
213 incorrectly calculated as an average bloom initiation date in July (e.g., day of year = 185), where the correct mean
214 is in January (e.g., day of year 3).

215



216
 217 Figure 1: Methodological flow chart outlining the steps taken to calculate the phytoplankton seasonal metrics. An
 218 example time-series illustrating the performance of the resulting phenological indices for a bimodal (double peak)
 219 bloom in the Southern Ocean (45°S, 7.5°W) is provided for the three different phenological methods, biomass-
 220 based threshold (TS), cumulative sum (CS) and rate of change (RC). *See Methodology for pre-processing steps.

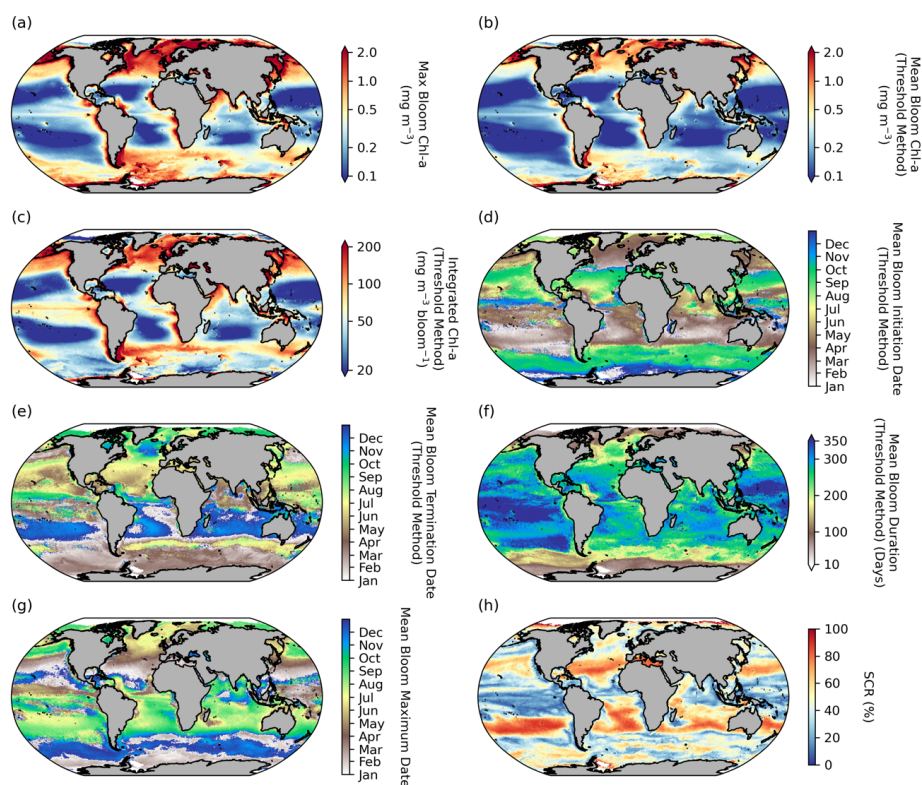
221 3 Results and Discussion

222 3.1 Global open-ocean phytoplankton seasonal metrics

223 A significant degree of regional variability is evident in the mean distribution of seasonal metrics (bloom
 224 amplitude, timing, and seasonality) (Figure 2). Bloom magnitude metrics (max bloom chl-a, mean bloom chl-a
 225 and integrated bloom chl-a; Figure 2a-c) are all higher in the high-latitudes and in the coastal regions, particularly
 226 in the Eastern Boundary Current Systems, and lowest in the oligotrophic subtropical gyres. There is a general
 227 equator-to-pole symmetry in the timing of phytoplankton blooms between the northern and southern hemispheres.



228 In the subpolar regions phytoplankton blooms initiate in the northern hemisphere during Boreal Spring to early
229 summer (March-May) and in the southern hemisphere in Austral Spring to early summer (September-November)
230 in response to light availability (Sverdrup, 1953) (Figure 2d). While in the subtropics, where there is ample light
231 throughout the year, blooms typically initiate in autumn to winter in response to nutrient supplies through winter-
232 driven deepening of the mixed-layer (Fauchereau et al., 2011; Thomalla et al., 2011). In both the Antarctic and
233 Arctic polar regions, phytoplankton blooms initiate in Austral (December) and Boreal summer (July), when the
234 sea-ice cover melts. The timing of bloom maximum follows the same equator-to-pole symmetry as bloom
235 initiation (Figure 2g), with high latitude regions peaking in Austral and Boreal summer, whereas the subtropics
236 peak in Austral and Boreal winter. This large-scale meridional structuring of the bloom timing is as expected and
237 similarly found in previous large-scale satellite based phenological studies (Sapiano et al., 2012; Kahru et al., 2011;
238 Racault et al., 2012). There is a larger degree of spatial heterogeneity in bloom termination (Figure 2e), particularly
239 evident in regions such as the high latitude North Atlantic and sub-Antarctic, with terminations that extend up to
240 6 months later in comparison to surrounding areas which were initiated at a similar time. This manifests in zonal
241 asymmetries across the different basins for bloom duration (Figure 2f), with considerably longer blooms occurring
242 in the Pacific basin compared with the Atlantic and Indian basins. SCR covers a large range of variability across
243 latitudinal bands. Notably, SCR (Figure 2h) is oftentimes low in regions where bloom duration is long, and this
244 relationship is strongest in the tropical Pacific ($r \sim -0.4$). In the Southern Ocean, long-sustained but highly variable
245 blooms were proposed as a response to intermittent physical forcing (high-frequency wind and meso to
246 submesoscale dynamics) that entrain nutrients and postpone the seasonal termination (Thomalla et al., 2011).



247

248 Figure 2: Global distribution of phytoplankton seasonal metrics. Mean [1998 – 2022] maps of (a) bloom max
249 chlorophyll (chl-a), (b) mean chl-a over bloom duration, (c) integrated chl-a over bloom duration, (d) bloom
250 initiation, (e) bloom termination, (f) bloom duration, (g) bloom max chl-a date, and (h) seasonal cycle
251 reproducibility (SCR). Phenological indices (b-f) are determined using the Biomass-based threshold method as
252 defined in Henson et al., 2018; Thomalla et al., 2023.

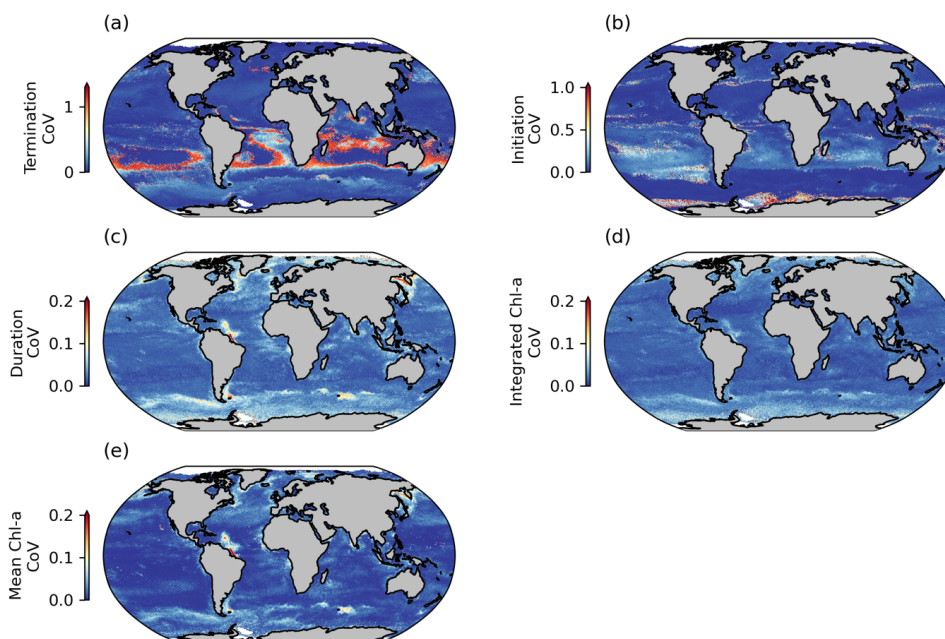
253 3.2 Comparison between phenology detection methods

254 Phytoplankton blooms can initiate rapidly, slowly, be short lived, intermittent, or sustained over a growing season,
255 with different detection methods being more or less sensitive to these varying characteristics of the seasonal bloom
256 (Thomalla et al., 2023; Brody et al., 2013). In this data product we have chosen to provide three methods of
257 application to all resolutions and allow the user to determine which method (or all) is most appropriate for their
258 region and application. For example, the TS method, based on the range of bloom amplitude (refer to methods),
259 may be more suitable for studies wanting to investigate the match or mismatch between phytoplankton and upper
260 trophic levels (explanation provided in Brody et al., (2013). The RC method, which identifies the bloom initiation
261 as the time when chl-a increases rapidly, is likely more suitable for investigating the physical or biochemical



262 mechanisms that create conditions in which the bloom occurs (Brody et al., 2013). Whereas the CS method could
263 be used to identify either of the features above (Brody et al., 2013). It is also interesting and potentially valuable
264 to determine when and where different methods of determination agree or disagree. The coefficient of variation
265 is used here to assess the agreement between climatological means from different methods of detection across
266 regional domains (with strong agreement represented by values closest to zero).

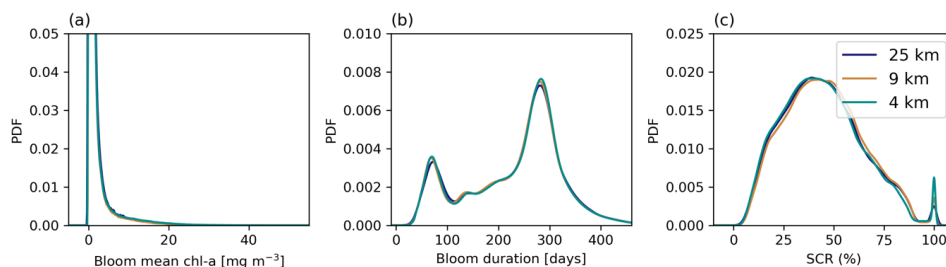
267 Across large regions of the global ocean, there is strong agreement between methodological approaches (Figure
268 3). The largest disagreements between phenological detection methods are in bloom termination (Figure 3a), with
269 the most notable differences evident in the boundaries of the southern hemisphere subtropical regions and of the
270 northern boundary of the subAntarctic zone. With bloom initiation, the largest difference in the detection methods
271 similarly occur in the southern hemisphere notably within the subtropical gyres and within the Antarctic Marginal
272 Ice Zone against the Antarctic continent where data is particularly sparse (Figure 3b). Dissonance is also evident
273 at the transition between the subtropical and subpolar Northern Hemisphere. This is not too surprising, given that
274 these boundaries represent areas of significant biogeochemical signatures and regime shifts between
275 phytoplankton seasonal characteristics with strong north-south gradients in bloom metrics (Figure 2). While there
276 are no other comparisons of these detection methods on a global scale, such differences were similarly seen in
277 (Brody et al., 2013) for the North Atlantic bloom, their Figure 4, where the largest differences between bloom
278 initiation methods occurred at the sharp transition boundaries between the subtropical and subpolar latitudes.
279 There is general agreement in bloom duration between the different methods (Figure 3c), with only a ~20-day
280 difference in the climatological global median between TS and the other methods, data not shown. Similarly, for
281 integrated and mean bloom chl-a (Figure 3d, e) there is in general little difference between the methods of
282 detection, with largest differences, as with duration, occurring in the Southern Ocean, particularly around sub-
283 Antarctic Islands, and a localised region of the Atlantic where the Amazon River discharges occurs.



284
285 Figure 3: Comparisons between phenological detection methods, the Threshold method (TC), the Cumulative
286 Sum method (CS) and the Relative Change method (RC), for selected seasonal phytoplankton bloom metrics,
287 including (a) bloom termination, (b) bloom initiation, (c) bloom duration, (d) bloom integrated chl-a and (e)
288 bloom mean chl-a. The coefficient of variation (CoV) is calculated as the inter-method standard deviation
289 normalised to the inter-method mean, please note the different scale in panels (a) and (b).

290 3.3. High-resolution phenology indices

291 The phenology data product presented here is offered at three different horizontal resolutions (4, 9 and 25 km),
292 which when compared on a global scale (Figure 4) shows little to no difference in the overall mean distribution
293 of three selected phytoplankton seasonal metrics, including bloom mean chl-a (Figure 4a), bloom duration (Figure
294 4b) and SCR (Figure 4c). Given that the large-scale distributions of the seasonal metrics remain virtually the same
295 there is little benefit for the user to use the more computationally expensive 4 km product for applications across
296 these larger scales.



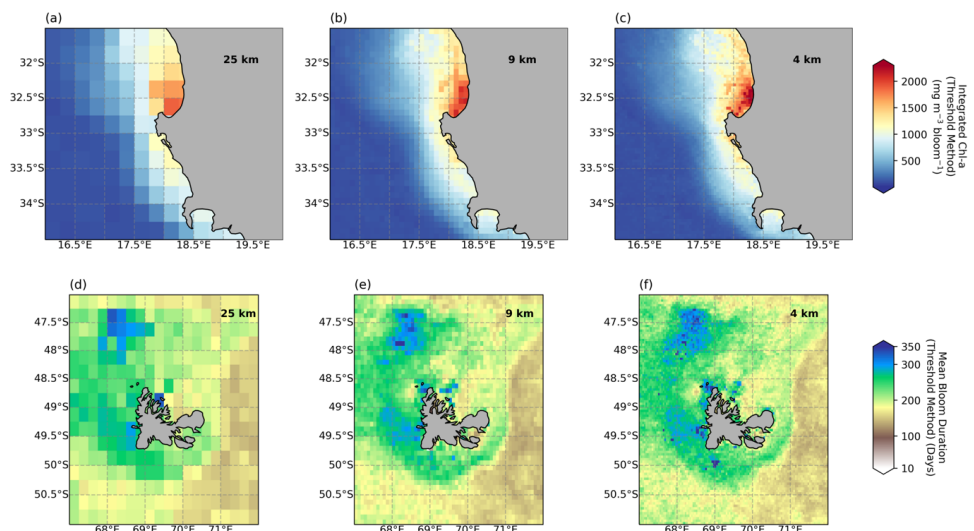
297

298 Figure 4: Probability Density Functions (PDF) of annual mean (calculated from 1998 to 2022) phytoplankton
299 seasonal cycle metrics, compared across three different spatial resolutions (4, 9 and 25 km) for (a) bloom mean
300 chlorophyll-a, (b) bloom duration and (c) seasonal cycle reproducibility (SCR). The TS phenology method is used
301 for (a) and (b).

302

303 There are, however, notable differences in the resolution of the product on smaller regional scales which appear
304 qualitatively different when compared at two example sites (Figure 5). The sites were selected to reflect regions
305 where a critical dependence is anticipated on the timing and magnitude of seasonal phytoplankton production.
306 The Benguela upwelling system (Figure 5a-c), off the west coast of South Africa is an essential region for
307 supporting key fisheries, while the subAntarctic Kerguelen Island (Figure 5d-f) is a vulnerable marine ecosystem
308 that supports a number of key species. The coarseness of the 25 km product is clearly evident in both sites at these
309 scales, it is considerably more pixelated and there are notable patches where there are differences in the resultant
310 phenological metric between resolutions. For example, in the near-shore of St Helena Bay the integrated bloom
311 chl-a climatology (2017-2022) differs between resolutions from 1654 mg m⁻³ bloom⁻¹, 1841 mg m⁻³ bloom⁻¹, and
312 1843 mg m⁻³ bloom⁻¹, for the 25 km, 9 km and 4 km maps respectively. At Kerguelen Island, interaction of the
313 Polar Front with shallow bathymetry generates persistent fine-scale ocean dynamics that set strong regional
314 gradients in phytoplankton production (Park et al., 2014). These fine-scale gradients are clearly seen in the spatial
315 variability of bloom duration captured by the higher resolution products. The ‘footprint’ of the island is evident
316 in the extended bloom durations occurring over the shallow plateau associated with the island where there is
317 considerable resuspension of dissolved iron, a key limiting nutrient (Blain et al., 2001). These examples highlight
318 how this data product can be applied to derive valuable indicators for use in national biodiversity assessments,
319 pelagic ecosystems mapping and marine resource management with the added potential of monitoring change in
320 climate sensitive regions relevant for ecosystem services. For regional studies or applications in coastal domains
321 it is recommended that users favour the high spatial resolution product, as it could facilitate detection of finer
322 scale delineations of phenoregions in transitional waters or detect fine scale distributions in phenology metrics
323 that are associated with physical or oceanographic features such as eddies, bays, and upwelling cells. While some
324 phenology indicators produced from daily data could offer additional insights into coastal regions with high
325 temporal variability (e.g., Ferreira et al., 2021), our dataset offers a resource for areas where long gaps in the time-
326 series could negate the use of daily data.

327



328

329 Figure 5: Regional domains comparing the impact of different resolutions (a,d) 25 km, (b,e) 9 km and (c,f) 4 km
330 on (a-c) bloom integrated chl-a and (d-f) the bloom duration averaged from 2017-2022 for (a-c) the Benguela
331 Upwelling System off the west coast of South Africa and (d-f) Kerguelen, a Sub-Antarctic island in the Southern
332 Ocean.

333 4 Data availability

334 The data are available on the Zenodo repository under the following DOIs, 4 km: 10.5281/zenodo.8402932, 9 km:
335 10.5281/zenodo.8402847 and 25 km: 10.5281/zenodo.8402823 (Nicholson et al., 2023a, b, c). Chl-a data, used to
336 develop the phytoplankton phenology product, is available from the Ocean Colour-CCI dataset (v.6.0) at
337 <https://esa-oceancolour-cci.org>.

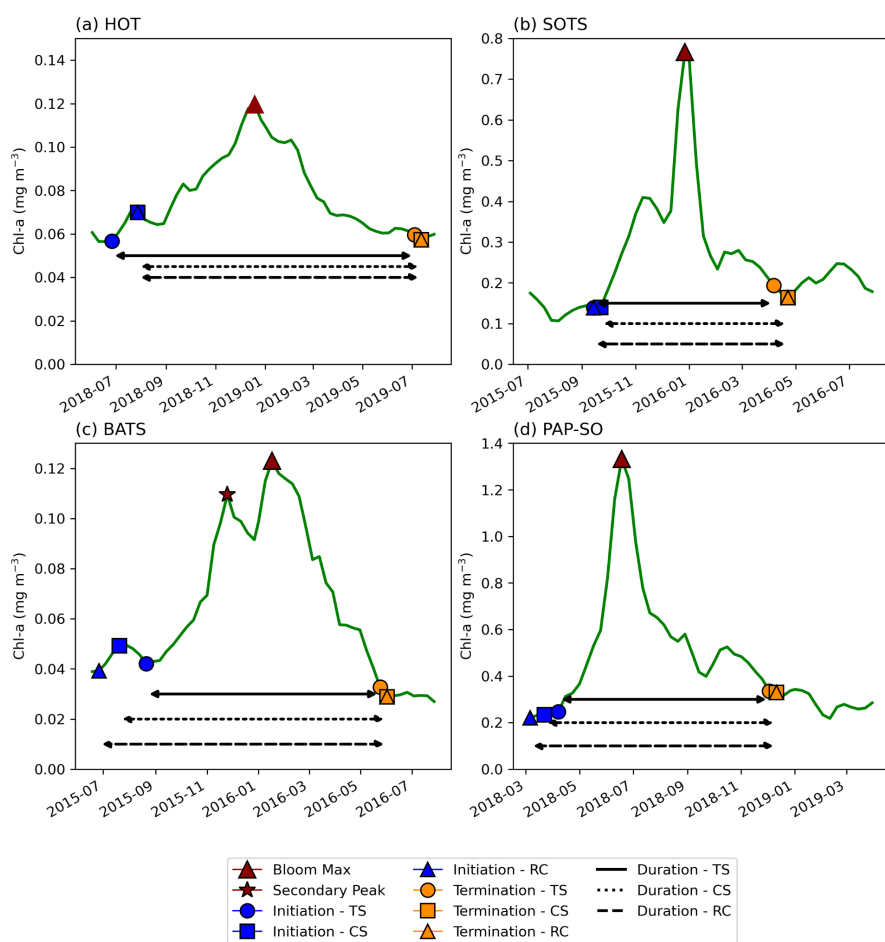
338 5 Conclusions

339 The data product presented here provides a 25-year continuous record of key phytoplankton seasonal cycle metrics
340 (phytoplankton bloom phenology, bloom seasonality and bloom magnitude) on a global-scale. It includes three
341 different phenology detection methods that are widely used by the community. We do not advocate for a particular
342 method over another, the strengths and weaknesses of these different approaches have been highlighted in other
343 studies (e.g., Brody et al., 2013), it is up to the user to choose which (if not all) is the most appropriate for their
344 research applications. The data product is also provided at three different horizontal resolutions (4, 9 and 25 km)
345 for regional versus global-scale application. This product is applicable for a broad range of national to international
346 research and industry applications. Its primary strength is that it can be used to assess, monitor, and understand
347 regional to global-scale characteristics in phytoplankton phenology and to detect change associated with
348 environmental drivers, which is critical for effective management of marine ecosystems and fisheries. This data



349 product will undergo regular updates for future applications and extended time series analysis, which typically
 350 happens every two years. It will also be updated when data is temporally extended or when the OC-CCI releases
 351 any version updates beyond v.6.0 that will include backwards corrections for previous years, so the entire dataset
 352 aligns with the latest version of OC-CCI. This proactive helps to prevent the retention of erroneous values within
 353 the data set.

354 **Appendix A**



355
 356

357 Figure A1: Examples of phytoplankton bloom seasonal cycles and comparisons in phenological detection
 358 methods at key sustained observing stations across the global ocean. For (a) Hawaii Ocean Time-series (HOT,
 359 $21^{\circ} 20.6'N$, $158^{\circ} 16.4'W$), (b) Southern Ocean Time Series Observatory (SOTS, $140^{\circ}E$, $47^{\circ}S$), (c) Bermuda
 360 Atlantic Time-series Study (BATS, $31^{\circ} 50' N$, $64^{\circ} 10'W$) and (d) Porcupine Abyssal Plain (PAP-SO, $49^{\circ}N$,
 361 $16.5^{\circ}W$) sustained observatory time-series.



362

363 **Author contributions.** Conceptualization: SN, TJRK, SJT. Formal analysis: SN, TJRK, MES, Software: TRJK,
364 SN, NC. Visualisations: SN, JRK. Writing – original draft: SN. Writing, reviewing, and editing: SN, TJRK, SJT,
365 MES, NC.

366 **Competing interests.** The contact author has declared that none of the authors has any competing interests.

367 **Acknowledgements**

368 We would like to acknowledge the OC-CCI group for providing the satellite data used in this manuscript. The
369 authors acknowledge their institutional support from the CSIR Parliamentary Grant (0000005278) and the
370 Department of Science and Innovation. We similarly acknowledge the Centre for High-Performance Computing
371 (NICIS-CHPC) for the support and computational hours required for the analysis of this work. SN, TRK, ST and
372 NC acknowledge the National Research Foundation (SANAP200324510487; SANAP200511521175;
373 MCR210429598142).

374 **References**

- 375 Barnes, D. K. A. and Barnes, D. K. A.: Blue Carbon on Polar and Subpolar Seabeds, Carbon Capture,
376 Utilization and Sequestration, <https://doi.org/10.5772/INTECHOPEN.78237>, 2018.
- 377 Bennington, V., McKinley, G. A., Dutkiewicz, S., and Ullman, D.: What does chlorophyll variability tell us
378 about export and air-sea CO₂ flux variability in the North Atlantic?, *Global Biogeochem Cycles*, 23,
379 <https://doi.org/10.1029/2008GB003241>, 2009.
- 380 Blain, S., Tréguer, P., Belviso, S., Bucciarelli, E., Denis, M., Desabre, S., Fiala, M., Martin Jézéquel, V., Le
381 Fèvre, J., Mayzaud, P., Marty, J. C., and Razouls, S.: A biogeochemical study of the island mass effect in the
382 context of the iron hypothesis: Kerguelen Islands, Southern Ocean, *Deep Sea Research Part I: Oceanographic*
383 *Research Papers*, 48, 163–187, [https://doi.org/10.1016/S0967-0637\(00\)00047-9](https://doi.org/10.1016/S0967-0637(00)00047-9), 2001.
- 384 Boot, A., von der Heydt, A. S., and Dijkstra, H. A.: Effect of Plankton Composition Shifts in the North Atlantic
385 on Atmospheric pCO₂, *Geophys Res Lett*, 50, e2022GL100230, <https://doi.org/10.1029/2022GL100230>, 2023.
- 386 Brody, S. R., Lozier, M. S., and Dunne, J. P.: A comparison of methods to determine phytoplankton bloom
387 initiation, *J Geophys Res Oceans*, 118, 2345–2357, <https://doi.org/10.1002/JGRC.20167>, 2013.
- 388 Buitenhuis, E. T., Hashioka, T., and Quéré, C. Le: Combined constraints on global ocean primary production
389 using observations and models, *Global Biogeochem Cycles*, 27, 847–858, <https://doi.org/10.1002/GBC.20074>,
390 2013.
- 391 Carr, M. E., Friedrichs, M. A. M., Schmeltz, M., Noguchi Aita, M., Antoine, D., Arrigo, K. R., Asanuma, I.,
392 Aumont, O., Barber, R., Behrenfeld, M., Bidigare, R., Buitenhuis, E. T., Campbell, J., Ciotti, A., Dierssen, H.,
393 Dowell, M., Dunne, J., Esaias, W., Gentili, B., Gregg, W., Groom, S., Hoepffner, N., Ishizaka, J., Kameda, T.,
394 Le Quéré, C., Lohrenz, S., Marra, J., Mélin, F., Moore, K., Morel, A., Reddy, T. E., Ryan, J., Scardi, M., Smyth,



- 395 T., Turpie, K., Tilstone, G., Waters, K., and Yamanaka, Y.: A Comparison of Global Estimates of Marine
396 Primary Production From Ocean Color, *Deep Sea Res 2 Top Stud Oceanogr*, 53, 741–770,
397 <https://doi.org/10.1016/j.dsr2.2006.01.028>, 2006.
- 398 Charlson, R. J., Lovelock, J. E., Andreae, M. O., and Warren, S. G.: Oceanic phytoplankton, atmospheric
399 sulphur, cloud albedo and climate, *Nature* 1987 326:6114, 326, 655–661, <https://doi.org/10.1038/326655a0>,
400 1987.
- 401 Cushing, D. H.: Plankton Production and Year-class Strength in Fish Populations: an Update of the
402 Match/Mismatch Hypothesis, *Adv Mar Biol*, 26, 249–293, [https://doi.org/10.1016/S0065-2881\(08\)60202-3](https://doi.org/10.1016/S0065-2881(08)60202-3),
403 1990.
- 404 Devries, T.: Annual Review of Environment and Resources The Ocean Carbon Cycle,
405 <https://doi.org/10.1146/annurev-environ-120920.2022>.
- 406 Falkowski, P. G.: The role of phytoplankton photosynthesis in global biogeochemical cycles, *Photosynth Res*,
407 39, 235–258, <https://doi.org/10.1007/BF00014586/METRICS>, 1994.
- 408 Fauchereau, N., Tagliabue, A., Bopp, L., and Monteiro, P. M. S.: The response of phytoplankton biomass to
409 transient mixing events in the Southern Ocean, *Geophys Res Lett*, 38, 1–6,
410 <https://doi.org/10.1029/2011GL048498>, 2011.
- 411 Ferreira, A., Brotas, V., Palma, C., Borges, C., and Brito, A. C.: Assessing Phytoplankton Bloom Phenology in
412 Upwelling-Influenced Regions Using Ocean Color Remote Sensing, *Remote Sensing* 2021, Vol. 13, Page 675,
413 13, 675, <https://doi.org/10.3390/RS13040675>, 2021.
- 414 Field, C. B., Behrenfeld, M. J., Randerson, J. T., and Falkowski, P.: Primary production of the biosphere:
415 Integrating terrestrial and oceanic components, *Science* (1979), 281, 237–240,
416 https://doi.org/10.1126/SCIENCE.281.5374.237/SUPPL_FILE/982246E_THUMB.GIF, 1998.
- 417 Gittings, J. A., Raitsos, D. E., Brewin, R. J. W., and Hoteit, I.: Links between Phenology of Large
418 Phytoplankton and Fisheries in the Northern and Central Red Sea, *Remote Sensing* 2021, Vol. 13, Page 231, 13,
419 231, <https://doi.org/10.3390/RS13020231>, 2021.
- 420 Harris, C. R., Millman, K. J., van der Walt, S. J., Gommers, R., Virtanen, P., Cournapeau, D., Wieser, E.,
421 Taylor, J., Berg, S., Smith, N. J., Kern, R., Picus, M., Hoyer, S., van Kerkwijk, M. H., Brett, M., Haldane, A.,
422 del Río, J. F., Wiebe, M., Peterson, P., Gérard-Marchant, P., Sheppard, K., Reddy, T., Weckesser, W., Abbasi,
423 H., Gohlke, C., and Oliphant, T. E.: Array programming with NumPy, *Nature* 2020 585:7825, 585, 357–362,
424 <https://doi.org/10.1038/s41586-020-2649-2>, 2020.
- 425 Henson, S. A., Sanders, R., Madsen, E., Morris, P. J., Le Moigne, F., and Quartly, G. D.: A reduced estimate of
426 the strength of the ocean’s biological carbon pump, <https://doi.org/10.1029/2011GL046735>, 2011.
- 427 Henson, S. A., Cole, H. S., Hopkins, J., Martin, A. P., and Yool, A.: Detection of climate change-driven trends
428 in phytoplankton phenology, *Glob Chang Biol*, 24, e101–e111, <https://doi.org/10.1111/gcb.13886>, 2018.
- 429 Kahru, M., Brotas, V., Manzano-Sarabia, M., and Mitchell, B. G.: Are phytoplankton blooms occurring earlier
430 in the Arctic?, *Glob Chang Biol*, 17, 1733–1739, <https://doi.org/10.1111/J.1365-2486.2010.02312.X>, 2011.
- 431 Koeller, P., Fuentes-Yaco, C., Platt, T., Sathyendranath, S., Richards, A., Ouellet, P., Orr, D., Skúladóttir, U.,
432 Wieland, K., Savard, L., and Aschan, M.: Basin-scale coherence in phenology of shrimps and phytoplankton in
433 the North Atlantic Ocean, *Science* (1979), 324, 791–793, <https://doi.org/10.1126/SCIENCE.1170987>, 2009.



- 434 Korhonen, H., Carslaw, K. S., Spracklen, D. V., Mann, G. W., and Woodhouse, M. T.: Influence of oceanic
435 dimethyl sulfide emissions on cloud condensation nuclei concentrations and seasonality over the remote
436 Southern Hemisphere oceans: A global model study, *Journal of Geophysical Research: Atmospheres*, 113,
437 15204, <https://doi.org/10.1029/2007JD009718>, 2008.
- 438 Longhurst, A., Sathyendranath, S., Platt, T., and Caverhill, C.: An estimate of global primary production in the
439 ocean from satellite radiometer data, *J Plankton Res*, 17, 1245–1271,
440 <https://doi.org/10.1093/PLANKT/17.6.1245>, 1995.
- 441 Lutz, M. J., Caldeira, K., Dunbar, R. B., and Behrenfeld, M. J.: Seasonal rhythms of net primary production and
442 particulate organic carbon flux to depth describe the efficiency of biological pump in the global ocean, *J*
443 *Geophys Res Oceans*, 112, 10011, <https://doi.org/10.1029/2006JC003706>, 2007.
- 444 McCoy, D. T., Burrows, S. M., Wood, R., Grosvenor, D. P., Elliott, S. M., Ma, P. L., Rasch, P. J., and
445 Hartmann, D. L.: Natural aerosols explain seasonal and spatial patterns of Southern Ocean cloud albedo, *Sci*
446 *Adv*, 1, https://doi.org/10.1126/SCIADV.1500157/SUPPL_FILE/1500157_SM.PDF, 2015.
- 447 Nicholson, S., Ryan-Keogh, T., Thomalla, S., Chang, N., and Smith, M.: Global Phytoplankton Phenological
448 Indices - 4km resolution, <https://doi.org/10.5281/zenodo.8402932>, October 2023a.
- 449 Nicholson, S., Ryan-Keogh, T., Thomalla, S., Chang, N., and Smith, M.: Global Phytoplankton Phenological
450 Indices - 9km resolution, <https://doi.org/10.5281/zenodo.8402847>, October 2023b.
- 451 Nicholson, S., Ryan-Keogh, T., Thomalla, S., Chang, N., and Smith, M.: Global Phytoplankton Phenological
452 Indices - 25km resolution, <https://doi.org/10.5281/zenodo.8402823>, October 2023c.
- 453 Nicholson, S. A., Lévy, M., Llorca, J., Swart, S., and Monteiro, P. M. S.: Investigation into the impact of storms
454 on sustaining summer primary productivity in the Sub-Antarctic Ocean, *Geophys Res Lett*, 43, 9192–9199,
455 <https://doi.org/10.1002/2016GL069973>, 2016.
- 456 Palevsky, H. I. and Quay, P. D.: Influence of biological carbon export on ocean carbon uptake over the annual
457 cycle across the North Pacific Ocean, *Global Biogeochem Cycles*, 31, 81–95,
458 <https://doi.org/10.1002/2016GB005527>, 2017.
- 459 Park, K. T., Yoon, Y. J., Lee, K., Tunved, P., Krejci, R., Ström, J., Jang, E., Kang, H. J., Jang, S., Park, J., Lee,
460 B. Y., Traversi, R., Becagli, S., and Hermansen, O.: Dimethyl Sulfide-Induced Increase in Cloud Condensation
461 Nuclei in the Arctic Atmosphere, *Global Biogeochem Cycles*, 35, e2021GB006969,
462 <https://doi.org/10.1029/2021GB006969>, 2021.
- 463 Park, Y. H., Durand, I., Kestenare, E., Rougier, G., Zhou, M., D'Ovidio, F., Cotté, C., and Lee, J. H.: Polar
464 Front around the Kerguelen Islands: An up-to-date determination and associated circulation of
465 surface/subsurface waters, *J Geophys Res Oceans*, 119, 6575–6592, <https://doi.org/10.1002/2014JC010061>,
466 2014.
- 467 Platt, T., White, G. N., Zhai, L., Sathyendranath, S., and Roy, S.: The phenology of phytoplankton blooms:
468 Ecosystem indicators from remote sensing, *Ecol Modell*, 220, 3057–3069,
469 <https://doi.org/10.1016/J.ECOLMODEL.2008.11.022>, 2009.
- 470 Racault, M. F., Le Quéré, C., Buitenhuis, E., Sathyendranath, S., and Platt, T.: Phytoplankton phenology in the
471 global ocean, *Ecol Indic*, 14, 152–163, <https://doi.org/10.1016/j.ecolind.2011.07.010>, 2012.



- 472 Racault, M. F., Sathyendranath, S., and Platt, T.: Impact of missing data on the estimation of ecological
473 indicators from satellite ocean-colour time-series, *Remote Sens Environ*, 152, 15–28,
474 <https://doi.org/10.1016/J.RSE.2014.05.016>, 2014.
- 475 Rogers, A. D., Frinault, B. A. V., Barnes, D. K. A., Bindoff, N. L., Downie, R., Ducklow, H. W., Friedlaender,
476 A. S., Hart, T., Hill, S. L., Hofmann, E. E., Linse, K., McMahon, C. R., Murphy, E. J., Pakhomov, E. A.,
477 Reygondeau, G., Staniland, I. J., Wolf-Gladrow, D. A., and Wright, R. M.: Antarctic Futures: An Assessment of
478 Climate-Driven Changes in Ecosystem Structure, Function, and Service Provisioning in the Southern Ocean,
479 <https://doi.org/10.1146/annurev-marine-010419-011028>, 12, 87–120, [https://doi.org/10.1146/ANNUREV-](https://doi.org/10.1146/ANNUREV-MARINE-010419-011028)
480 [MARINE-010419-011028](https://doi.org/10.1146/ANNUREV-MARINE-010419-011028), 2020.
- 481 Rolinski, S., Horn, H., Petzoldt, T., and Paul, L.: Identifying cardinal dates in phytoplankton time series to
482 enable the analysis of long-term trends, *Oecologia*, 153, 997–1008, <https://doi.org/10.1007/S00442-007-0783-2>,
483 2007.
- 484 Sapiano, M. R. P., Brown, C. W., Schollaert Uz, S., and Vargas, M.: Establishing a global climatology of
485 marine phytoplankton phenological characteristics, *J Geophys Res Oceans*, 117,
486 <https://doi.org/10.1029/2012JC007958>, 2012.
- 487 Sathyendranath, S., Brewin, R. J. W., Brockmann, C., Brotas, V., Calton, B., Chuprin, A., Cipollini, P., Couto,
488 A. B., Dingle, J., Doerffer, R., Donlon, C., Dowell, M., Farman, A., Grant, M., Groom, S., Horseman, A.,
489 Jackson, T., Krasemann, H., Lavender, S., Martinez-Vicente, V., Mazeran, C., Mélin, F., Moore, T. S., Müller,
490 D., Regner, P., Roy, S., Steele, C. J., Steinmetz, F., Swinton, J., Taberner, M., Thompson, A., Valente, A.,
491 Zühlke, M., Brando, V. E., Feng, H., Feldman, G., Franz, B. A., Frouin, R., Gould, R. W., Hooker, S. B., Kahru,
492 M., Kratzer, S., Mitchell, B. G., Muller-Karger, F. E., Sosik, H. M., Voss, K. J., Werdell, J., and Platt, T.: An
493 Ocean-Colour Time Series for Use in Climate Studies: The Experience of the Ocean-Colour Climate Change
494 Initiative (OC-CCI), *Sensors* 2019, Vol. 19, Page 4285, 19, 4285, <https://doi.org/10.3390/S19194285>, 2019.
- 495 Sathyendranath, S., Jackson, T., Brockmann, C., Brotas, V., Calton, B., Chuprin, A., Clements, O., Cipollini, P.,
496 Danne, O., Dingle, J., Donlon, C., Grant, M., Groom, S., Krasemann, H., Lavender, S., Mazeran, C., Mélin, F.,
497 Müller, D., Steinmetz, F., Valente, A., Zühlke, M., Feldman, G., Franz, B., Frouin, R., Werdell, J., and Platt, T.:
498 ESA Ocean Colour Climate Change Initiative (Ocean_Colour_cci): Global chlorophyll-a data products gridded
499 on a sinusoidal projection, Version 5.0., NERC EDS Centre for Environmental Data Analysis,
500 <https://doi.org/10.5285/1dbe7a109c0244aaad713e078fd3059a>, 2021.
- 501 Seyboth, E., Groch, K. R., Dalla Rosa, L., Reid, K., Flores, P. A. C., and Secchi, E. R.: Southern Right Whale
502 (*Eubalaena australis*) Reproductive Success is Influenced by Krill (*Euphausia superba*) Density and Climate,
503 *Scientific Reports* 2016 6:1, 6, 1–8, <https://doi.org/10.1038/srep28205>, 2016.
- 504 Stock, C. A., John, J. G., Rykaczewski, R. R., Asch, R. G., Cheung, W. W. L., Dunne, J. P., Friedland, K. D.,
505 Lam, V. W. Y., Sarmiento, J. L., and Watson, R. A.: Reconciling fisheries catch and ocean productivity, *Proc*
506 *Natl Acad Sci U S A*, 114, E1441–E1449,
507 https://doi.org/10.1073/PNAS.1610238114/SUPPL_FILE/PNAS.1610238114.SM01.MOV, 2017.
- 508 Sverdrup, H. U.: On Conditions for the Vernal Blooming of Phytoplankton, *ICES Journal of Marine Science*,
509 18, 287–295, <https://doi.org/10.1093/ICESJMS/18.3.287>, 1953.



510 Thomalla, S. J., Fauchereau, N., Swart, S., and Monteiro, P. M. S.: Regional scale characteristics of the seasonal
511 cycle of chlorophyll in the Southern Ocean, *Biogeosciences*, 8, 2849–2866, [https://doi.org/10.5194/bg-8-2849-](https://doi.org/10.5194/bg-8-2849-2011)
512 2011, 2011.

513 Thomalla, S. J., Nicholson, S. A., Ryan-Keogh, T. J., and Smith, M. E.: Widespread changes in Southern Ocean
514 phytoplankton blooms linked to climate drivers, *Nature Climate Change* 2023 13:9, 13, 975–984,
515 <https://doi.org/10.1038/s41558-023-01768-4>, 2023.

516 Tweddle, J. F., Gubbins, M., and Scott, B. E.: Should phytoplankton be a key consideration for marine
517 management?, *Mar Policy*, 97, 1–9, <https://doi.org/10.1016/J.MARPOL.2018.08.026>, 2018.

518 Virtanen, P., Gommers, R., Oliphant, T. E., Haberland, M., Reddy, T., Cournapeau, D., Burovski, E., Peterson,
519 P., Weckesser, W., Bright, J., van der Walt, S. J., Brett, M., Wilson, J., Millman, K. J., Mayorov, N., Nelson, A.
520 R. J., Jones, E., Kern, R., Larson, E., Carey, C. J., Polat, İ., Feng, Y., Moore, E. W., VanderPlas, J., Laxalde, D.,
521 Perktold, J., Cimrman, R., Henriksen, I., Quintero, E. A., Harris, C. R., Archibald, A. M., Ribeiro, A. H.,
522 Pedregosa, F., van Mulbregt, P., Vijaykumar, A., Bardelli, A. Pietro, Rothberg, A., Hilboll, A., Kloeckner, A.,
523 Scopatz, A., Lee, A., Rokem, A., Woods, C. N., Fulton, C., Masson, C., Häggström, C., Fitzgerald, C.,
524 Nicholson, D. A., Hagen, D. R., Pasechnik, D. V., Olivetti, E., Martin, E., Wieser, E., Silva, F., Lenders, F.,
525 Wilhelm, F., Young, G., Price, G. A., Ingold, G. L., Allen, G. E., Lee, G. R., Audren, H., Probst, I., Dietrich, J.
526 P., Silterra, J., Webber, J. T., Slavič, J., Nothman, J., Buchner, J., Kulick, J., Schönberger, J. L., de Miranda
527 Cardoso, J. V., Reimer, J., Harrington, J., Rodríguez, J. L. C., Nunez-Iglesias, J., Kuczynski, J., Tritz, K.,
528 Thoma, M., Neville, M., Kümmerer, M., Bolingbroke, M., Tartre, M., Pak, M., Smith, N. J., Nowaczyk, N.,
529 Shebanov, N., Pavlyk, O., Brodtkorb, P. A., Lee, P., McGibbon, R. T., Feldbauer, R., Lewis, S., Tygier, S.,
530 Sievert, S., Vigna, S., Peterson, S., More, S., Pudlik, T., et al.: SciPy 1.0: fundamental algorithms for scientific
531 computing in Python, *Nature Methods* 2020 17:3, 17, 261–272, <https://doi.org/10.1038/s41592-019-0686-2>,
532 2020.

533 Yamaguchi, R., Rodgers, K. B., Timmermann, A., Stein, K., Schlunegger, S., Bianchi, D., Dunne, J. P., and
534 Slater, R. D.: Trophic level decoupling drives future changes in phytoplankton bloom phenology, *Nature*
535 *Climate Change* 2022 12:5, 12, 469–476, <https://doi.org/10.1038/s41558-022-01353-1>, 2022.

536 Zhuang, J., dussin, raphael, Huard, D., Bourgault, P., Banihirwe, A., Raynaud, S., Malevich, B., Schupfner, M.,
537 Filipe, Levang, S., Gauthier, C., Jüling, A., Almansi, M., RichardScottOZ, RondeauG, Rasp, S., Smith, T. J.,
538 Stachelek, J., Plough, M., Pierre, Bell, R., Caneill, R., and Li, X.: pangeo-data/xESMF: v0.8.2,
539 <https://doi.org/10.5281/zenodo.8356796>, September 2023.

540
541